

2-Phenylpyrazolo[4,3-*d*]pyrimidin-7-one as a New Scaffold To Obtain Potent and Selective Human A₃ Adenosine Receptor Antagonists: New Insights into the Receptor–Antagonist Recognition[†]

Ombretta Lenzi,[‡] Vittoria Colotta,^{*,‡} Daniela Catarzi,[‡] Flavia Varano,[‡] Daniela Poli,[‡] Guido Filacchioni,[‡] Katia Varani,[§] Fabrizio Vincenzi,[§] Pier Andrea Borea,[§] Silvia Paoletta,[⊥] Erika Morizzo,[⊥] and Stefano Moro^{*,⊥}

[‡]Dipartimento di Scienze Farmaceutiche, Laboratorio di Progettazione, Sintesi e Studio di Eterocicli Biologicamente Attivi, Università di Firenze, Polo Scientifico, Via Ugo Schiff, 6, 50019 Sesto Fiorentino, Italy, [§]Dipartimento di Medicina Clinica e Sperimentale, Sezione di Farmacologia, Università di Ferrara, Via Fossato di Mortara 17-19, 44100 Ferrara, Italy, and [⊥]Molecular Modeling Section (MMS), Dipartimento di Scienze Farmaceutiche, Università di Padova, Via Marzolo 5, 35131 Padova, Italy

Received May 27, 2009

A molecular simplification approach of previously reported 2-arylpyrazolo[3,4-*c*]quinolin-4-ones was applied to design 2-arylpyrazolo[4,3-*d*]pyrimidin-7-one derivatives as new human A₃ adenosine receptor antagonists. Substituents with different lipophilicity and steric hindrance were introduced at the 5-position of the bicyclic scaffold (R₅ = H, Me, Et, Ph, CH₂Ph) and on the 2-phenyl ring (OMe, Me). Most of the synthesized derivatives were highly potent hA₃ adenosine receptor antagonists, the best being the 2-(4-methoxyphenyl)pyrazolo[4,3-*d*]pyrimidin-7-one (K_i = 1.2 nM). The new compounds were also highly selective, being completely devoid of affinity toward hA₁, hA_{2A}, and hA_{2B} adenosine receptors. On the basis of the recently published human A_{2A} receptor crystallographic information, we propose a novel receptor-driven hypothesis to explain both A₃ AR affinity and A₃ versus A_{2A} selectivity profiles of these new antagonists.

Introduction

The neuromodulator adenosine affects a wide variety of physiopathological processes through activation of four G-protein-coupled receptors (GPCRs⁶), classified as A₁, A_{2A}, A_{2B}, and A₃ subtypes.^{1,2} Activation of adenosine receptors (ARs) can induce inhibition (A₁ and A₃) or activation (A_{2A} and A_{2B}) of the adenylate cyclase.¹ Moreover, other second messenger signaling pathways can be associated with stimulation of ARs. The A₃ AR positively modulates phospholipase C³ and D,⁴ K_{ATP} channel,⁵ inositol triphosphate, and intracellular calcium.^{5,6} Activation of this receptor subtype leads to modulation of mitogen-activated protein kinases (MAPK), such as the extracellular signal-regulated kinase (ERK) 1/2 and the stress-activated protein kinase p38.⁷ What is known about A₃-signaling in several processes is still controversial. The A₃ regulation of the cell cycle may induce cell protection or cell

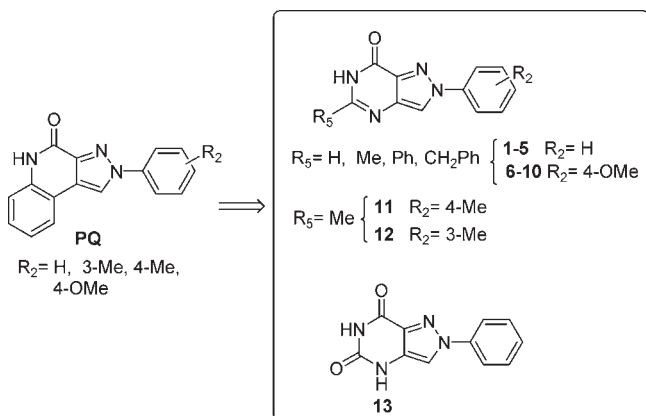
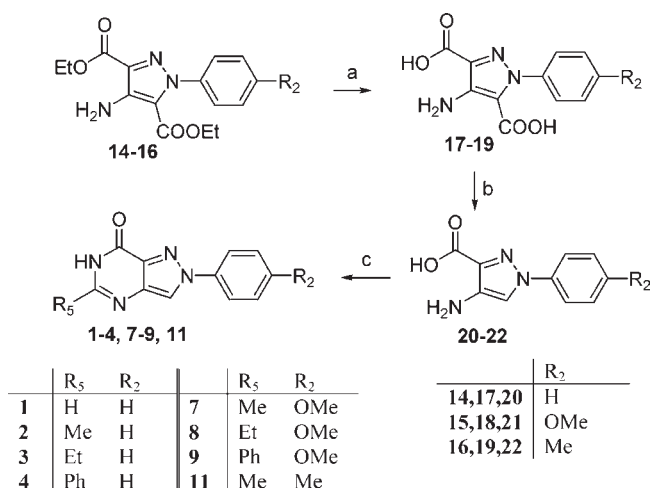
death, depending on the degree of receptor activation and/or the cell type or the toxic insult.^{7–9} As a consequence of this dual effect, both A₃ receptor agonists and antagonists might be effective therapeutics in cancer.^{9–11} In the brain and in other tissues, such as kidney, lung, and eye, activation of the A₃ AR may induce both pro- and antisurvival effects, thus affording either protection or damage, depending on the situation.⁹ In the immune system, the A₃-mediated effects can be either proinflammatory or antiinflammatory,⁹ depending on the investigated models. Thus, even though it is clear that the A₃ AR is involved in many disease pathways, much remains to be clarified about its role. Therefore, the search for new selective A₃ AR ligands, either agonists or antagonists, continues to be attractive.

In our laboratory, we have directed much effort toward the study of human (h) A₃ AR antagonists belonging to different classes of heteroaromatic systems.^{12–20} Of these, we have identified a class of tricyclic hA₃ antagonists, the pyrazolo[3,4-*c*]quinolin-4-one (PQ) derivatives (Chart 1).^{13,17} The PQ derivatives show high affinities for the hA₃ receptor (K_i = 3–30 nM) and also high hA₃ versus hA_{2A} selectivity, since they do not bind the hA_{2A} receptor. They possess quite good affinities for the hA₁ AR and scarce hA₃ versus hA₁ selectivity. Thus, to develop a new class of compounds targeting the A₃ receptor, but with a better selectivity profile, we performed a molecular simplification of the PQ structure to yield the 2-arylpyrazolo[4,3-*d*]pyrimidin-7-one derivatives **1–12** (Chart 1). Substituents with different lipophilicity and steric hindrance were introduced at the 5-position of the 2-phenylpyrazolopyrimidin-7-one scaffold (R₅ = H, Me, Et, Ph, CH₂Ph) to give compounds **1–5**. Certain substituents that were profitable for hA₃ affinity and selectivity in the PQ lead series were introduced on the 2-phenyl ring. In particular, a 4-methoxy group was

[†]The authors are deeply honored to contribute to this special Centennial issue, and they are also extremely grateful to the Division of Medicinal Chemistry of the American Chemical Society for its outstanding support toward the advancement of medicinal chemistry.

*To whom correspondence should be addressed. For V.C.: phone, +39 055 4573731; fax, +39 055 4573780; e-mail, vittoria.colotta@unifi.it. For S.M.: phone, +39 049 8275704; fax, +39 049 8275366; e-mail, stefano.moro@unipd.it.

^aAbbreviations: GPCRs, G-protein-coupled receptors; AR, adenosine receptor; MAPK, mitogen-activated protein kinase; ERK, extracellular signal-regulated kinase; h, human; NECA, 5'-(*N*-ethylcarboxamido)adenosine; cAMP, cyclic adenosine monophosphate; Cl-IB-MECA, 2-chloro-*N*⁶-(3-iodobenzyl)-5'-(*N*-methylcarbamoyl)adenosine; DPCPX, 8-cyclopentyl-1,3-dipropylxanthine; ZM-241385, 4-(2-[7-amino-2-(2-furyl)-[1,2,4]triazolo[2,3-*d*][1,3,5]triazin-5-ylamino]ethyl)phenol; I-AB-MECA, *N*⁶-(4-amino-3-iodobenzyl)-5'-(*N*-methylcarbamoyl)adenosine; SAR, structure–affinity relationship; TM, transmembrane; rmsd, root-mean-square deviation; EL2, second extracellular loop; MOE, Molecular Operating Environment software.

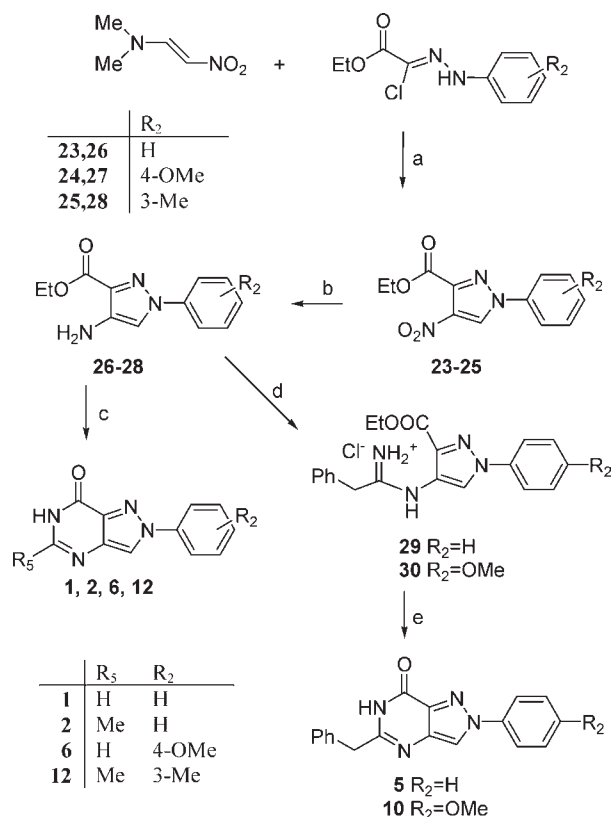
Chart 1. Molecular Simplification Approach from the Pyrazolo[3,4-*c*]quinolin-4-one to the Pyrazolo[4,3-*d*]pyrimidin-7-one Scaffold**Scheme 1^a**

^a (a) 20% KOH/EtOH; (b) 85% H₃PO₄; (c) R₅-C(OEt)₃, NH₄OAc, microwave irradiation.

appended on the 2-phenyl ring of derivatives **1–5** to afford compounds **6–10**. 3-Methyl or 4-methyl groups were also inserted on the 2-phenyl ring of the 5-methyl derivative **2** (compounds **11** and **12**, respectively). Finally, an oxo function was introduced at the 5-position to give the 2-phenylpyrazolo[4,3-*d*]pyrimidin-5,7-dione **13**. We propose a novel receptor-driven hypothesis to explain both the hA₃ affinity and hA₃ versus A_{2A} receptor selectivity profiles of these new antagonists. This is based on the recently published structure of the hA_{2A} AR, in conjunction with the high affinity hA_{2A} AR antagonist 4-(2-[7-amino-2-(2-furyl)[1,2,4]-triazolo[2,3-*a*]-[1,3,5]triazin-5-ylamino]ethyl)phenol (ZM-241385).²¹

Chemistry

The 5-substituted 2-arylpyrazolo[4,3-*d*]pyrimidin-7-one derivatives **1–12** were prepared following two synthetic pathways, as depicted in Schemes 1 and 2. Scheme 1 shows the synthesis of compounds **1–4**, **7–9**, and **11** starting from ethyl 4-amino-1-arylpyrazole-3,5-dicarboxylates **14–16** which were prepared as previously described.^{22–24} Compounds **14–16** were hydrolyzed to the corresponding 4-amino-1-arylpyrazole-3,5-dicarboxylic acids **17–19** which were heated at 100 °C in 85% phosphoric acid to be transformed

Scheme 2^a

^a (a) NEt₃, CHCl₃; (b) H₂, Pd/C; (c) R₅-C(OEt)₃, NH₄OAc, microwave irradiation; (d) R₅-CH₂-CN, HCl_g, anhydrous dioxane; (e) neat, T = 230 °C.

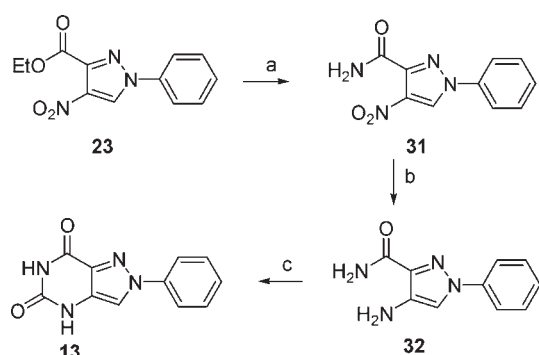
into the 4-amino-1-arylpyrazole-3-carboxylic acids **20–22**. These latter derivatives were cyclized with suitable triethyl orthoesters and ammonium acetate via one-pot three-component reaction and under solvent-free conditions. The reaction, performed under microwave irradiation, afforded the desired 5-substituted 1-arylpyrazolo[4,3-*d*]pyrimidin-7(6*H*)-ones **1–4**, **7–9**, and **11**. Since the yields in this last step were quite low (from 18% to 40%), a new synthetic pathway was followed to obtain the target bicyclic derivatives **5**, **6**, **10**, and **12** (Scheme 2). Compounds **1** and **2** were also resynthesized to evaluate whether the second synthetic method was better than the previous one. Allowing *N,N*-dimethyl-2-nitroethaneamine²⁵ to react with suitable ethyl *N*₁-arylhydrazono-*N*₂-chloroacetates,^{26,27} in refluxing chloroform and in the presence of triethylamine, the ethyl 1-aryl-4-nitropyrazole-3-carboxylates **23–25** were obtained. The 4-nitro-substituted compounds **23–25** were reduced to the corresponding 4-amino derivatives **26–28** which were cyclized with triethyl orthoesters and ammonium acetate, under microwave irradiation, to give the 1-arylpyrazolo[4,3-*d*]pyrimidines **1**, **2**, **6**, **12**. Interestingly, compounds **1** and **2** were obtained with significantly higher yields (about 70%) than those obtained by the above-described cyclization of derivative **20**. Intermediates **26** and **27** were also reacted with benzyl cyanide, in anhydrous dioxane and hydrogen chloride, to give the ethyl 4-(2-phenylacetamidoimido)-1-arylpyrazole-3-carboxylate hydrochlorides **29** and **30** which were heated at 250 °C to provide the corresponding 1-aryl-5-benzylpyrazolo[4,3-*d*]pyrimidin-7(6*H*)-ones **5** and **10**. Finally, Scheme 3 describes the synthesis of the 2-phenylpyrazolo[4,3-*d*]pyrimidin-5,7-dione **13**. Reaction of

ethyl 4-nitro-1-phenylpyrazole-3-carboxylate **23** with saturated aqueous solution of ammonia yielded the 4-nitro-1-phenyl-3-carboxamide **31**, which was catalytically reduced to give the corresponding 4-amino derivative **32**.²² The bicyclic derivative **13** was obtained by allowing compound **32** to react with triphosgene.

Pharmacological Assays

The synthesized derivatives **1–13** were tested to evaluate their affinity at hA₁, hA_{2A}, and hA₃ ARs. Compounds were also tested at the hA_{2B} AR subtype by measuring their inhibitory effects on NECA-stimulated cAMP levels in CHO cells stably transfected with the hA_{2B} AR. Finally, the antagonistic potency of all the pyrazolopyrimidin-7-one derivatives able to bind at the hA₃ AR (**1–3**, **5–8**, **10–12**) was assessed by evaluating their effect on Cl-IB-MECA-inhibited

Scheme 3^a



^a (a) 33% aqueous NH₃; (b) H₂, 10% Pd/C, EtOH; (c) triphosgene, NEt₃, anhydrous tetrahydrofuran.

cAMP production in CHO cells, stably expressing hA₃ ARs. All pharmacological data are collected in Table 1, together with those of ZM-241385, taken as a reference compound.

Results and Discussion

The binding results indicate that the herein reported molecular simplification of the PQ structure was successful, since it not only maintained high affinity for the hA₃ AR but also increased the hA₃ selectivity. Indeed, most of the newly synthesized compounds displayed hA₃ AR affinities in the low nanomolar range ($K_i = 1.2–72$ nM) and are totally inactive at the other three investigated ARs. Structure–affinity relationship (SAR) analysis shows that both R₂ and R₅ substituents play a key role in anchoring to the hA₃ receptor site. Both the lipophilicity and steric hindrance of the R₅ substituent are critical for hA₃ affinity. Compound **1**, bearing a hydrogen atom at the 5-position, shows a good hA₃ affinity ($K_i = 185$ nM) which was significantly enhanced when the 5-hydrogen atom was replaced by a 5-ethyl moiety (compound **3**) or, even better, by a 5-methyl group (compound **2**). The presence at the 5-position of the bulkier phenyl ring was detrimental, with derivative **4** showing a null hA₃ binding activity. Replacement of the 5-phenyl group with a 5-benzyl moiety restored the hA₃ AR affinity (compound **5**). However, it was significantly lower than those of the less hindered 5-substituted derivatives **1–3**. These results indicate that the presence of a quite small lipophilic substituent at the 5-position of the pyrazolo[4,3-*d*]pyrimidin-7-one scaffold is important. This is probably because this group engages hydrophobic bonds with a lipophilic receptor pocket of limited size. The presence of a substituent on the 2-phenyl ring (R₂) was also a crucial feature of these new hA₃ AR

Table 1. Binding Affinity (K_i) at hA₁, hA_{2A}, and hA₃ ARs and Potency (IC₅₀) at hA_{2B} and hA₃ ARs

	R ₅	R ₂	binding experiments, K_i (nM) or I (%)			cAMP assays, IC ₅₀ (nM) or I (%)	
			hA ₃ ^a	hA ₁ ^b	hA _{2A} ^c	hA _{2B} ^d	hA ₃ ^e
1	H	H	185 ± 19	1%	1%	3%	725 ± 64
2	Me	H	16 ± 2	9%	1%	2%	87 ± 9
3	Et	H	52 ± 5	11%	6%	1%	245 ± 23
4	Ph	H	10%	22%	10%	4%	
5	Ph-CH ₂	H	900 ± 95	11%	1%	4%	6%
6	H	4-OMe	54 ± 6	2%	1%	3%	270 ± 26
7	Me	4-OMe	1.2 ± 0.1	5%	1%	2%	5.2 ± 0.5
8	Et	4-OMe	14 ± 2	1%	1%	5%	63 ± 7
9	Ph	4-OMe	16%	1%	1%	5%	
10	Ph-CH ₂	4-OMe	250 ± 27	10%	1%	4%	850 ± 76
11	Me	4-Me	10 ± 1	1%	1%	4%	46 ± 5
12	Me	3-Me	72 ± 8	4%	1%	2%	354 ± 33
13			12%	4%	5%	2%	
ZM-241385			5%	180 ± 16	1.2 ± 0.2	42 ± 5	2%

^a Displacement of specific [¹²⁵I]AB-MECA binding to hA₃CHO cells, where K_i values are mean values ± SEM of four separate assays each performed in duplicate. Percentage of inhibition in [¹²⁵I]AB-MECA competition binding assays to hA₃CHO cells at 1 μM tested compounds. ^b Percentage of inhibition in [³H]DPCPX competition binding assays to hA₁CHO cells at 1 μM tested compounds. ^c Percentage of inhibition in [³H]ZM241385 competition binding assays to hA_{2A}CHO cells at 1 μM tested compounds. ^d Percentage of inhibition on cAMP experiments in hA_{2B}CHO cells, stimulated by 200 nM NECA, at 1 μM examined compounds. ^e IC₅₀ values are expressed as mean values ± SEM of four separate cAMP experiments in hA₃CHO cells, inhibited by 100 nM Cl-IB-MECA.

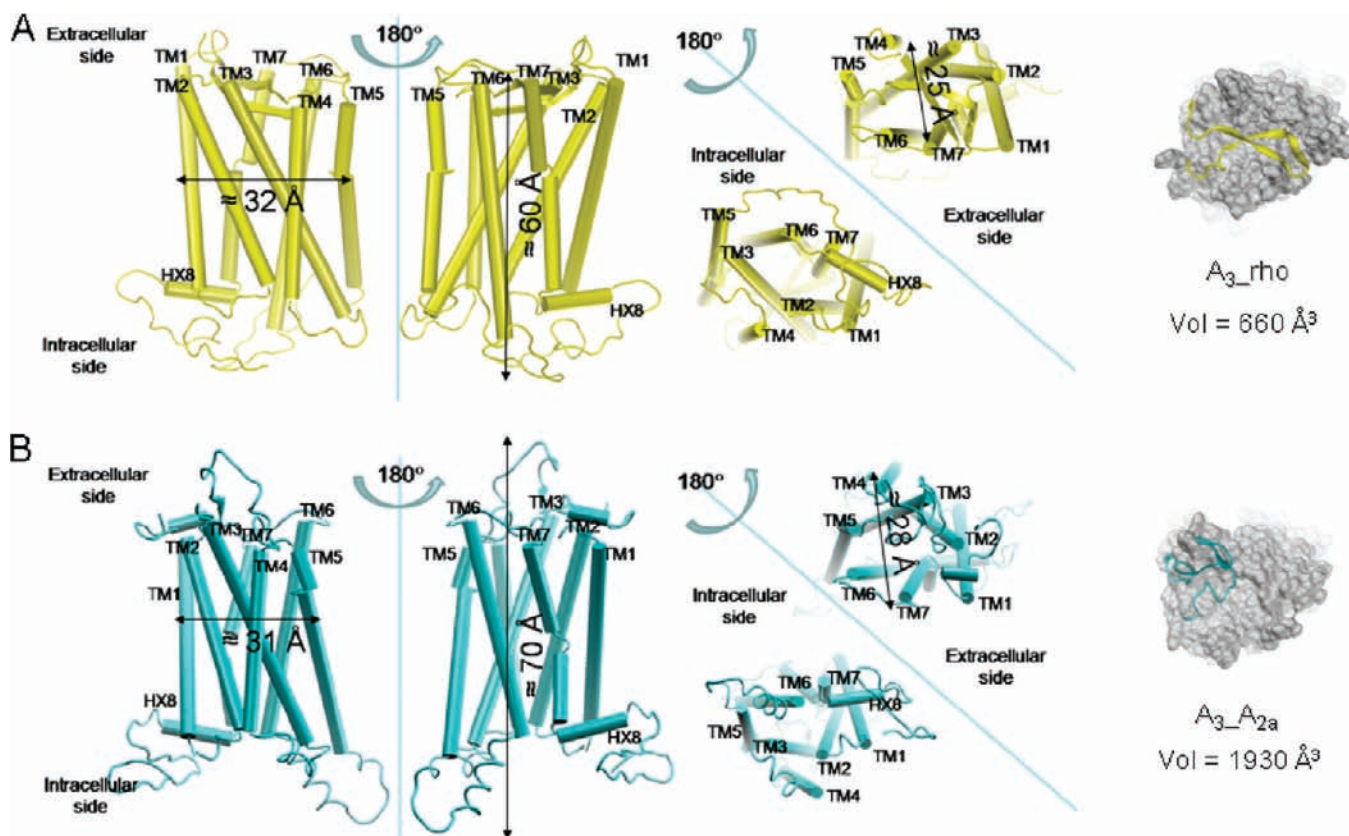


Figure 1. Topology of the hA₃ AR built using bovine rhodopsin (A) and human A_{2A} AR (B) as templates. The molecular surfaces and the calculated volumes refer to the ligand binding pockets.

Table 2. Root Mean Square Deviation (rmsd) of the Backbone of the Aligned Models of the hA₃AR Compared with the Available Crystallographic Templates^a

	all TMs	all loops	TM1	TM2	TM3	TM4	TM5	TM6	TM7	HX8	EL2
rmsd (Å) with Respect to the hA ₃ AR Model from Bovine Rhodopsin (Backbone)											
A3_A2A	2.43	10.06	2.55	2.40	2.78	2.45	2.85	2.02	2.04	1.64	14.30
rmsd (Å) with Respect to the hA ₃ AR Model from hβ ₂ -Adrenergic Receptor (Backbone)											
A3_rho	2.29	10.86	2.82	2.12	1.98	2.01	2.07	2.19	1.85	3.73	11.44
A3_A2A	2.57	7.46	3.84	1.89	2.02	1.73	2.09	2.71	2.23	3.66	6.18

^aThe main difference among the models is due to the loops, which represent the most variable region of the templates and consequently of the models. Particular attention has to be given to EL2 because it is part of the binding pocket and it can directly interact with ligands.

antagonists. When a 4-methoxy group was introduced on the 2-phenyl ring of compounds **1–5**, a significant enhancement of the hA₃ affinity was obtained (compounds **6, 8–10**). Among the 2-(4-methoxyphenyl) derivatives **6–10**, the 5-methylsubstituted compound **7** emerged as the most active ($K_i = 1.2$ nM), confirming that the best substituent for the 5-position was the methyl group. Thus, taking **2** as the lead derivative, we tested two further substituents on the 2-phenyl ring because in the tricyclic PQ series they afforded the highest hA₃ AR affinities, i.e., the 4-Me and 3-Me groups (compounds **11** and **12**). Both compounds **11** and **12** show high hA₃ affinity, in particular the 2-(4-methylphenyl)-substituted compound **11** ($K_i = 10$ nM), but the 4-methoxy substituted derivative **7** remains the best in terms of hA₃ affinity. Finally, introduction of an oxo function at the 5-position of the pyrazolo[4,3-*d*]pyrimidin-7-one nucleus exerted a deleterious effect, with compound **13** displaying null affinity for the hA₃ receptor. All the new derivatives **1–3, 5–8, 10–12** were antagonists at the hA₃ AR. They show inhibitory

effects on Cl-IB-MECA-inhibited cAMP production, and their potencies are coherent with their hA₃ affinity values.

Molecular Modeling Studies

The recently published structure of the hA_{2A} AR, in conjunction with the high affinity antagonist ZM-241385, provides a new template for GPCR modeling, particularly for ARs.²¹ Therefore, we built a new homology model of the hA₃ AR using the crystal structure of the hA_{2A} receptor (PDB code 3EML) as a template (methodological details are summarized in the Experimental Section).

The helical arrangement is similar to the previously published rhodopsin-based homology models as shown in Figure 1.^{14–18,20} However, the transmembrane (TM) helices are slightly shifted, and the differences among their relative positions result in a root-mean-square deviation (rmsd) around 2.50 Å for the backbone atoms. A detailed comparison of the superimposed models is presented in Table 2, in which we report the values of rmsd for each TM helix. As seen

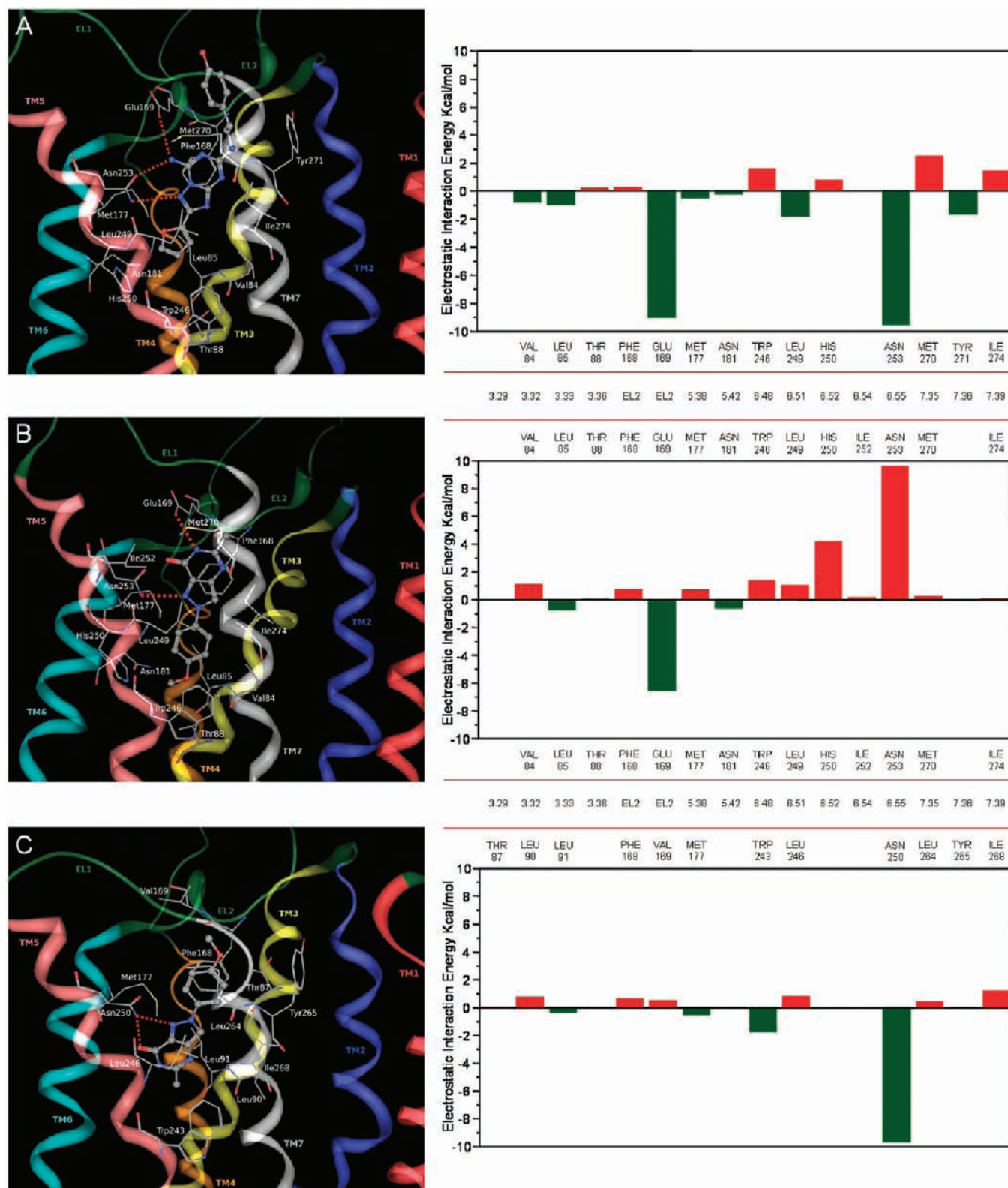


Figure 2. (A) Crystallographic binding mode of ZM-241385 inside the hA_{2A} receptor (PDB code 3EML) and hypothetical binding mode of compound 7 obtained after docking simulations (B) inside the hA_{2A} AR binding site and (C) inside the hA₃ AR binding site. Side chains of some amino acids important for ligand recognition and H-bonding interactions are highlighted. Hydrogen atoms are not displayed. Beside each pose, the graph displays the electrostatic interaction energy (in kcal/mol) between the ligand and each single amino acid involved in ligand recognition.

with the templates, the main difference between the two models of the hA₃ AR is in the loop region. The ligand binding pocket of the crystal structure of the hA_{2A} AR is shifted closer

to TM6 and TM7, and the position of the hA_{2A} AR antagonist is closer to these helices (Figure 2, panel A on the left).²¹ Important interactions are also established with the second

Table 3. Comparison of Different Molecular Docking Protocols in the Reproduction of the Binding Mode of ZM-241385 at the hA_{2A} AR^a

docking protocol	best rmsd (Å)	best ranked pose rmsd (Å)	mean poses rmsd (Å)	number of poses with rmsd < 2.5 Å
MOE tabu search	1.61	3.35	5.65	4/25
MOE simulated annealing	2.17	4.36	6.47	1/25
MOE genetic algorithm	2.25	9.06	6.66	2/25
GOLD (GoldScore)	0.63	1.95	1.20	25/25
GOLD (ChemScore)	1.31	3.90	3.13	11/25
GOLD (asp)	0.61	4.96	1.50	23/25
GLIDE	0.79	2.71	6.82	7/25
PLANTS (chemplp)	0.93	1.98	6.96	3/25
PLANTS (plp)	0.84	1.93	6.70	6/25
PLANTS (plp95)	1.97	11.80	8.22	4/25

^a Different scoring functions for the same protocol are reported in parentheses if available.

extracellular loop (EL2), in particular with Glu169. Indeed, the position of ZM-241385 is significantly different from that of 11-*cis*-retinal into the bovine rhodopsin²⁹ or of carazolol into the human β_2 -adrenergic receptor.³⁰ Even though GPCRs share a common topology, ligands may bind in a different fashion and interact with different positions of the receptor. The model built starting from the hA_{2A} AR template is different from previous models of the hA₃ AR; the binding pocket is closer to TM6 and TM7 and open to the extracellular side. Because of the open conformation to the extracellular side of the EL2, the volume of the binding site, estimated as $\sim 1930 \text{ \AA}^3$, was larger than the volume of the binding site of the rhodopsin-based model ($\sim 660 \text{ \AA}^3$), as summarized in Figure 1.

Although the hA₃ AR possesses a higher percentage of identity with the A_{2A} subtype than with the previously reported rhodopsin and β_2 -adrenergic structures, the conformations of the EL2 and, consequently, of the binding pocket of the hA₃ AR might be different from those of the hA_{2A} AR. The peculiarity of the hA_{2A} AR is the presence of three disulfide bridges on EL2, which are not conserved among ARs. Moreover, one additional disulfide bridge is present in the crystal structure of the hA_{2A} AR between Cys259 and Cys262 on EL3. Human A₃ and A_{2B} ARs do not present cysteine residues in the same positions, and the link cannot be formed in these two receptor subtypes. According to the alignment of the sequences, the hA₁AR presents two cysteines (Cys260 and Cys263) in the corresponding positions of the cysteines of the hA_{2A}AR. The formation of the disulfide bond is possible, but mutagenesis analysis showed that mutation of cysteine residues to alanine or serine does not change the affinity for agonists or antagonists.³¹ An in-depth investigation using lipid membrane molecular dynamics simulations is underway in our laboratory to verify the influence of EL2 conformation in the antagonist recognition process.

Starting from this novel hA₃AR model, a molecular modeling study was performed on the new 2-arylpyrazolo[4,3-*d*]pyrimidin-7-one derivatives **1–13** to identify the hypothetical binding mode at the hA₃ adenosine receptor and to rationalize the observed structure–activity relationships. In particular, molecular docking studies were carried out on both hA₃ and hA_{2A} adenosine receptors. As reported in the Experimental Section, four different programs were used to calibrate our docking protocol using the crystallographic pose of ZM-241385 into the hA_{2A} receptor as a reference (Table 3). On the basis of the lowest average ligand rmsd value obtained from the different docking algorithms, we decided to use Gold as a docking program for the pose inspection of the novel 2-arylpyrazolo[4,3-*d*]pyrimidin-7-one derivatives in both hA_{2A} and hA₃ receptors.

From the docking simulation analysis, almost all the derivatives were seen to share a similar binding pose in the TM

region of the hA₃ AR. Ligand recognition occurs in the upper region of the TM bundle, and the pyrazolo[4,3-*d*]pyrimidin-7-one scaffold is surrounded by TMs 3, 5, 6, 7 with the 2-phenyl ring pointing toward EL2 and the substituent at the 5-position (R₅) oriented toward the intracellular environment.

Figure 2 (panel C on the left) shows the hypothetical binding mode of compound **7**, which possesses the highest hA₃ affinity among all the newly synthesized derivatives (hA₃ AR K_i = 1.2 nM). This compound is anchored, inside the binding cleft, by two stabilizing hydrogen-bonding interactions with the amide moiety of Asn250 (6.55) side chain. The two hydrogen bonds involve the carbonyl group at the 7-position and one of the N atoms of the pyrazole ring, respectively. The asparagine residue 6.55, conserved among all AR subtypes, was already found to be important for ligand binding at both the hA₃ and hA_{2A} ARs.^{32,33} Compound **7** also forms hydrophobic interactions with many residues of the binding cleft including Leu90 (3.32), Leu91 (3.33), Phe168 (EL2), Val169 (EL2), Met177 (5.38), Trp243 (6.48), Leu246 (6.51), Leu264 (7.35), Tyr265 (7.36), Ile268 (7.39). In particular, the 2-phenyl ring forms an aromatic π – π stacking interaction with Phe168 (EL2), while the pyrazolo[4,3-*d*]pyrimidin-7-one core interacts with the highly conserved Trp243 (6.48), an important residue in receptor activation and in antagonist binding.³³

The 2-arylpyrazolo[4,3-*d*]pyrimidin-7-one derivatives bearing nonbulky moieties at the 5-position, such as 5-hydrogen atom (compounds **1** and **6**), 5-methyl group (compounds **2**, **11**, and **12**), and 5-ethyl group (compounds **3** and **8**), show a similar binding mode compared to compound **7**. In fact, for all these derivatives, the pyrazolo[4,3-*d*]pyrimidin-7-one core is perfectly aligned inside the TM region of the hA₃ receptor. In particular, the two hydrogen bonds with Asn250 (6.55), the aromatic stacking interaction with Phe168 (EL2), and the hydrophobic interaction with Trp243 (6.48) are conserved.

In contrast, binding poses of compounds bearing bulkier substituents, including 5-phenyl and 5-benzyl groups (compounds **4**, **5**, **9**, and **10**), are quite different. The 2-phenyl ring of these compounds is directed toward the intracellular environment rather than toward EL2, while the substituent at the 5-position (R₅) points toward TM2. Because of this different orientation of the molecule inside the binding cleft, these derivatives lose one of the two H-bonding interactions with Asn250 (6.55) and the π – π stacking interaction between Phe168 (EL2) and the 2-phenyl ring (data not shown). The lack of these important interactions seems to be why derivatives with bulky R₅ groups show low or null hA₃ AR affinities.

Compound **13** (bearing an oxo function at the 5-position) shows a completely different docking pose inside the hA₃ binding pocket, compared to all the other derivatives, and its

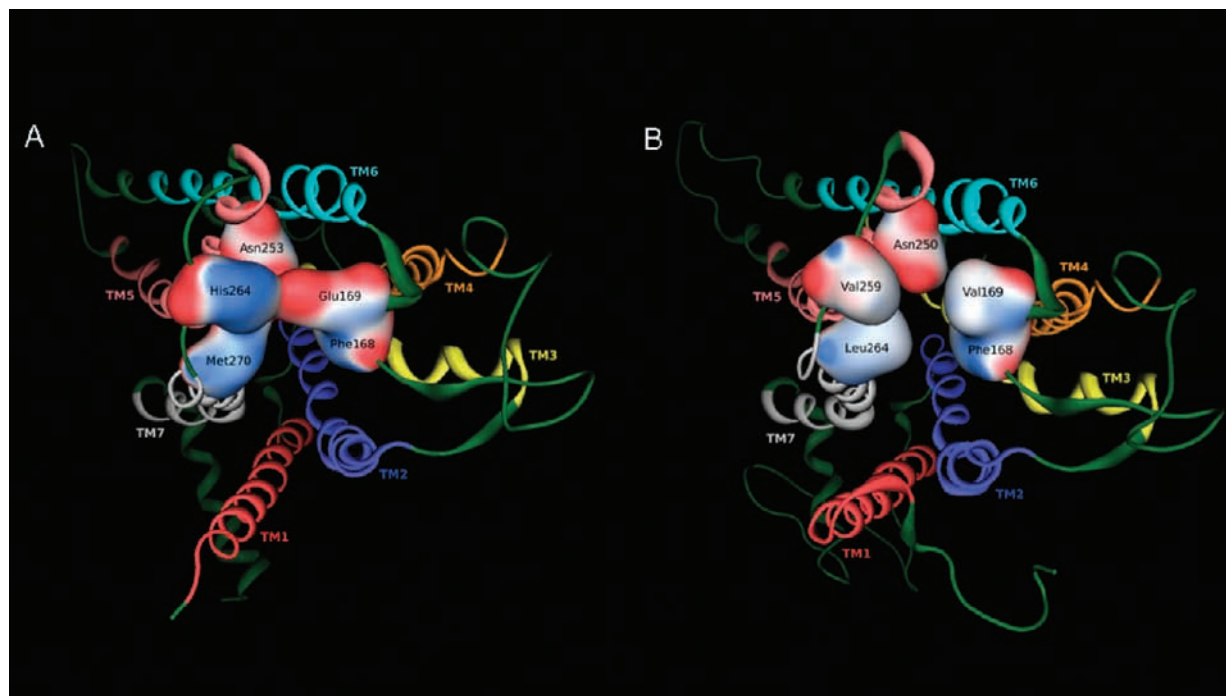


Figure 3. Access to the binding pocket of hA_{2A} (A) and hA₃ (B) ARs. Receptors are viewed from the extracellular side. Gaussian surface of some important amino acids is displayed. Surface color shows a screened electrostatic potential (where scale parameters are as follows: red, -35 kcal/mol; white, 0 kcal/mol; blue, $+35$ kcal/mol).

orientation is almost parallel to the membrane plane. Even though this molecule forms two H-bonding interactions with Asn250 (6.55), it is too far to interact with Trp243 (6.48), and so it loses the interaction with this important residue (data not shown).

With regard to the presence of a substituent on the 2-phenyl ring (R_2), it emerged that small groups (methyl and methoxy) enhance the hA₃ affinity even though they do not seem to be involved in particular interactions with residues of the binding pocket. Nevertheless, these substituents, because of their electron-donating properties, could reinforce the π - π stacking interaction of the 2-phenyl ring with the receptor. In addition, the methyl and methoxy groups increase the topological complementarity of the compounds with the TM binding cavity.

As shown in Figure 2 (panel B on the left), the hypothetical binding pose of compound **7**, obtained after molecular docking to the crystal structure of the hA_{2A} receptor, is quite different compared to the pose of the same compound on the hA₃ subtype (Figure 2, panel C on the left), although ligand recognition occurs in the same region of the TM bundle. In particular, the 2-phenyl ring points toward the intracellular environment and the substituent at the 5-position (R_5) is oriented toward EL2. The molecule forms two H-bonds, with Asn253 (6.55) and Glu169 (EL2), and an aromatic interaction with Phe168 (EL2).

All the newly synthesized derivatives **1–13** show this same binding mode inside the hA_{2A} receptor pocket. Although the predicted binding affinities are lower with respect to those estimated for the corresponding binding to the hA₃ receptor (around 3 – 9 kcal/mol), this only partially justifies the absence of A_{2A} binding observed experimentally. To analyze the possible ligand–receptor recognition mechanism in a more quantitative way, we calculated the individual electrostatic contribution ($\Delta E_{\text{int}}^{\text{el}}$) to the interaction energy (ΔE_{int}) of each receptor residue (see Experimental Section for more details).

From this study, one of the most critical residues affecting the affinity at ARs seems to be the asparagine 6.55 (Asn253 in hA_{2A} and Asn250 in hA₃). In particular, Asn253 is responsible for two stabilizing interactions with ZM-241385 into human A_{2A} AR. This is confirmed by the electrostatic contribution of around -10 kcal/mol to the whole interaction energy. Considering the binding poses of compound **7**, the electrostatic contribution of this asparagine residue to the interaction energy is completely different between hA_{2A} and hA₃ receptors (see Figure 2, panels B and C on the right, respectively). Asn250 (6.55) strongly stabilizes the ligand–hA₃ receptor complex (negative electrostatic interaction energy) because of the two hydrogen bonding interactions, while Asn253 (6.55) destabilizes the ligand–hA_{2A} receptor complex (positive electrostatic interaction energy). This detrimental contribution to the stability of the complex is due to the electrostatic repulsion between the oxo moiety of the pyrazolo[4,3-*d*]pyrimidin-7-one nucleus and the carbonyl group of Asn253 side chain. This could considerably reduce the permanence of these 2-aryl-pyrazolo[4,3-*d*]pyrimidin-7-one analogues in the TM binding pocket and explain the null affinity of these new derivatives for the hA_{2A} AR ($I = 1$ – 10%).

Moreover, comparing the docking pose of compound **7** on the hA_{2A} receptor with the crystallographic pose of the antagonist ZM-241385, we note that the bicyclic core of the pyrazolo[4,3-*d*]pyrimidin-7-one derivative is almost aligned with the bicyclic region of ZM-241385. Nevertheless, the exocyclic amino group (H-bond donor) of ZM-241385 is replaced with a carbonyl group (H-bond acceptor) in compound **7**, and this could lead to the substantially different affinities at the hA_{2A} receptor (see Table 1). The values of the electrostatic contributions to the binding energies are also coherent with this recognition scenario. Therefore, in the 7–hA_{2A} receptor complex, Glu169 (EL2) is the only amino acid that has a notable negative electrostatic interaction energy. Site-directed mutagenesis studies have shown that

this glutamate residue is important for ligand binding at the hA_{2A} AR.³⁴

We note that Glu169 (EL2) of the hA_{2A} receptor subtype is not present in the corresponding position of the hA₃ receptor, where the residue is replaced by a valine (Val169). This difference could influence not only the binding mode but also the entrance of ligands to the TM region of the receptors. As shown in Figure 3, the electrostatic potentials of amino acids present at the binding pocket entrance from the extracellular site are very different in the two receptors. In the hA₃ AR, the binding pocket gate is surrounded essentially by side chains of hydrophobic residues including Phe168 (EL2), Val169 (EL2), Ile253 (6.58), Val259 (EL3), Leu264 (7.35) (Figure 3B). In the hA_{2A} AR, there are ionic residues, such as Glu169 (EL2) and His264 (EL3) among the amino acids delimiting the binding site access (Figure 3A). We speculate that the presence of this charged gate may affect both the ligand orientation, while approaching the binding pocket, and its accommodation into the final TM binding cleft. Several studies are in progress in our laboratories to experimentally support our hypothesis.

Conclusion

The present study identifies a new class of highly potent and selective hA₃ AR antagonists, the 2-arylpyrazolo[4,3-*d*]-pyridine-7-one derivatives, which were designed as simplified analogues of our previously reported hA₃ antagonists. To depict the binding mode of these new hA₃ antagonists, we built a novel model of the hA₃ receptor, based on the recently published structure of the hA_{2A} receptor. This new A₃ receptor model can correctly interpret the SAR observed for the new antagonists in terms of both hA₃ affinity and hA₃ versus hA_{2A} selectivity. Moreover, we propose a very preliminary hypothesis concerning the specific roles of a few crucial amino acids in affecting the molecular mechanism of both the ligand-entering process and the TM-recognition process.

Experimental Section

(A) Chemistry. The microwave-assisted syntheses were performed using an Initiator EXP Biotage microwave instrument (frequency of irradiation: 2.45 GHz). Silica gel plates (Merck F₂₅₄) and silica gel 60 (Merck, 70–230 mesh) were used for analytical and column chromatography, respectively. All melting points were determined on a Gallenkamp melting point apparatus. Microanalyses were performed with a Perkin-Elmer 260 elemental analyzer for C, H, N, and the results were within $\pm 0.4\%$ of the theoretical values, unless otherwise stated. The IR spectra were recorded with a Perkin-Elmer Spectrum RX I spectrometer in Nujol mulls and are expressed in cm⁻¹. The ¹H NMR spectra were obtained with a Bruker Avance 400 MHz instrument. The chemical shifts are reported in δ (ppm) and are relative to the central peak of the solvent which was always DMSO-*d*₆. The following abbreviations are used: s = singlet, d = doublet, t = triplet, m = multiplet, br = broad, and ar = aromatic protons.

General Procedure for the Synthesis of 4-Amino-1-arylpyrazole-3,5-dicarboxylic Acids 17–19. A suspension of ethyl 4-amino-1-arylpyrazole-3,5-dicarboxylates **14–16**^{22–24} (1.64 mmol) in 20% KOH ethanolic solution (15 mL) was heated at 80 °C for 15 min. The mixture was cooled at room temperature and acidified at pH 2 with 12 N HCl. The solid was collected by filtration, washed with water, and recrystallized.

17: yield 50%; mp 198–200 °C (EtOH) (lit. mp 197–199 °C).²²

18: yield 55%; mp 180–182 °C (acetonitrile/MeOH); ¹H NMR 3.82 (s, 3H, OMe), 6.99 (d, 2H, ar, *J* = 8.5 Hz), 7.35 (d, 2H, ar, *J* = 8.5 Hz). Anal. (C₁₂H₁₁N₃O₅) C, H, N.

19: yield 52%; mp 243–245 °C (acetonitrile/MeOH); ¹H NMR 2.37 (s, 3H, Me), 7.25 (d, 2H, ar, *J* = 8.3 Hz), 7.30 (d, 2H, ar, *J* = 8.3 Hz). Anal. (C₁₂H₁₁N₃O₄) C, H, N.

General Procedure for the Synthesis of 4-Amino-1-arylpyrazole-3-carboxylic Acids 20–22. A suspension of 4-amino-1-arylpyrazole-3,5-dicarboxylic acids **17–19** in 85% H₃PO₄ was heated at 100 °C for 45 min. After cooling at room temperature, the solution was alkalized to pH 4–5 with 40% NaOH solution. The solid that precipitated was collected by filtration, washed with a few drops of water, and recrystallized.

20: yield 60%; mp 225–226 °C (EtOH) (lit. mp 223–225 °C).²²

21: yield 58%; mp 208–210 °C (EtOAc/EtOH); ¹H NMR 3.80 (s, 3H, OMe), 7.04 (d, 2H, ar, *J* = 8.9 Hz), 7.69–7.71 (m, 3H, 2ar + H5). Anal. (C₁₁H₁₁N₃O₃) C, H, N.

22: yield 55%; mp 213–214 °C (EtOAc/EtOH); ¹H NMR 2.33 (s, 3H, Me), 7.29 (d, 2H, ar, *J* = 8.3 Hz), 7.66 (d, 2H, ar, *J* = 8.3 Hz), 7.76 (s, 1H, H5). Anal. (C₁₁H₁₁N₃O₂) C, H, N.

General Procedure for the Synthesis of 5-Substituted 2-Arylpyrazolo[4,3-*d*]pyrimidin-7(6*H*)-ones 1–4, 7–9, 11. A mixture of 4-amino-1-arylpyrazole-3-carboxylic acids **20–22** (2.5 mmol), ammonium acetate (3.2 mmol), and the suitable orthoesters (3.2 mmol) was microwave-irradiated at 150 °C for 15 min. The suspension was cooled at room temperature, the solid was collected by filtration, washed with water and diethyl ether, and recrystallized. The crude compound **11** was purified by column chromatography (eluting system CH₂Cl₂/MeOH, 9:1) and then recrystallized.

1: yield 25%; mp 299–300 °C (acetonitrile); ¹H NMR 7.47 (t, 1H, ar, *J* = 7.3 Hz), 7.60 (t, 2H, ar, *J* = 7.3 Hz), 7.86 (s, 1H, H5), 8.03 (d, 2H, ar, *J* = 7.8 Hz), 9.14 (s, 1H, H3), 12.00 (br s, 1H, NH); IR 1673, 1724, 3170. Anal. (C₁₁H₈N₄O) C, H, N.

2: yield 18%; mp > 300 °C (2-methoxyethanol); ¹H NMR 2.31 (s, 3H, Me), 7.46 (t, 1H, ar, *J* = 7.4 Hz), 7.59 (t, 2H, ar, *J* = 7.4 Hz), 8.01 (d, 2H, ar, *J* = 8.0 Hz), 8.98 (s, 1H, H3), 11.92 (s, 1H, NH); IR 1683. Anal. (C₁₂H₁₀N₄O) C, H, N.

3: yield 30%; mp 270–272 °C (2-methoxyethanol); ¹H NMR 1.22 (t, 3H, Me, *J* = 7.5 Hz), 2.61 (q, 2H, CH₂, *J* = 7.5 Hz), 7.46 (t, 1H, ar, *J* = 7.3 Hz), 7.57–7.61 (m, 2H, ar), 8.01 (d, 2H, ar, *J* = 8.1 Hz), 9.02 (s, 1H, H3), 11.89 (br s, 1H, NH); IR 1688, 3150. Anal. (C₁₃H₁₂N₄O) C, H, N.

4: yield 30%; mp > 300 °C (2-methoxyethanol); ¹H NMR 7.47–7.65 (m, 6H, ar), 8.05 (d, 2H, ar, *J* = 7.7 Hz), 8.10 (d, 2H, ar, *J* = 7.8 Hz), 9.20 (s, 1H, H3), 12.26 (br s, 1H, NH); IR 1684, 3155. Anal. (C₁₇H₁₂N₄O) C, H, N.

7: yield 25%; mp > 300 °C (2-methoxyethanol); ¹H NMR 2.30 (s, 3H, Me), 3.80 (s, 3H, OMe), 7.11 (d, 2H, ar, *J* = 9.0 Hz), 7.92 (d, 2H, ar, *J* = 9.0 Hz), 8.87 (s, 1H, H3), 11.67 (br s, 1H, NH); IR 1678. Anal. (C₁₃H₁₂N₄O₂) C, H, N.

8: yield 25%; mp 278–280 °C (EtOH); ¹H NMR 1.22 (t, 3H, Me, *J* = 7.5 Hz), 2.59 (q, 2H, CH₂, *J* = 7.5 Hz), 3.84 (s, 3H, OMe), 7.13 (d, 2H, ar, *J* = 8.9 Hz), 7.91 (d, 2H, ar, *J* = 8.9 Hz), 8.91 (s, 1H, H3), 11.83 (br s, 1H, NH); IR 1702. Anal. (C₁₄H₁₄N₄O₂) C, H, N.

9: yield 18%; mp 291–293 °C (2-methoxyethanol); ¹H NMR 3.85 (s, 3H, OMe), 7.16 (d, 2H, ar, *J* = 7.0 Hz), 7.51–7.57 (m, 3H, ar), 7.97 (d, 2H, ar, *J* = 7.0 Hz), 8.11 (d, 2H, ar, *J* = 7.7 Hz), 9.09 (s, 1H, H3), 12.19 (br s, 1H, NH); IR 1681, 3180. Anal. (C₁₈H₁₄N₄O₂) C, H, N.

11: yield 23%; mp > 300 °C (MeOH/EtOH) ¹H NMR 2.31 (s, 3H, Me), 2.38 (s, 3H, Me), 7.39 (d, 2H, ar, *J* = 8.3 Hz), 7.89 (d, 2H, ar, *J* = 8.3 Hz), 8.91 (s, 1H, H3), 11.86 (br s, 1H, NH); IR 1685. Anal. (C₁₃H₁₂N₄O) C, H, N.

General Procedure for the Synthesis of Ethyl 1-Aryl-5-nitropyrazole-3-carboxylates 23–25. A solution of *N,N*-dimethyl-2-nitroethaneamine²⁵ (5.5 mmol), suitable ethyl *N*₁-arylhydrazono-*N*₂-chloroacetates^{26,27} (11 mmol), and triethylamine (11 mmol) in chloroform (30 mL) was refluxed for 48 h. After the mixture was cooled at room temperature, the solvent was evaporated at reduced pressure to give a residue which was taken up with ethanol (about 20 mL) to give crude compounds **23** and **24**, which were collected by filtration. To obtain derivative **25**, the residue was treated with

cyclohexane/EtOAc, the solid was filtered off, and the solvents were evaporated at reduced pressure. The solid obtained was purified by column chromatography (eluting system, EtOAc).

23: yield 45%; mp 149–150 °C (EtOH) (lit. 150–151 °C).²⁸

24: yield 25%; mp 91–92 °C (diethyl ether/petroleum ether 40–60 °C); ¹H NMR 1.33 (t, 3H, Me, *J* = 7.1 Hz), 3.83 (s, 3H, MeO), 4.41 (q, 2H, CH₂, *J* = 7.1 Hz), 7.13 (d, 2H, ar, *J* = 6.9 Hz), 7.85 (d, 2H, ar, *J* = 6.9 Hz), 9.61 (s, 1H, H5). Anal. (C₁₃H₁₃N₃O₅) C, H, N.

25: yield 40%; mp 118–120 °C (diethyl ether); ¹H NMR 1.33 (t, 3H, Me, *J* = 7.1 Hz), 2.41 (s, 3H, Me), 4.43 (q, 2H, CH₂, *J* = 7.1 Hz), 7.31 (d, 1H, ar, *J* = 7.6 Hz), 7.47 (t, 1H, ar, *J* = 7.8 Hz), 7.74 (d, 1H, ar, *J* = 8.1 Hz), 7.81 (s, 1H, ar), 9.70 (s, 1H, H5). Anal. (C₁₃H₁₃N₃O₄) C, H, N.

General Procedure for the Synthesis of Ethyl 4-Amino-1-arylpyrazole-3-carboxylates 26–28. The nitro derivatives **23–25** (3 mmol) were dissolved in a suitable solvent (**23** in boiling ethanol, 100 mL; **24** and **25** in EtOAc, 30 mL), and 10% Pd/C (10% p/p) was added to the solution. The mixture was hydrogenated in a Parr apparatus at 35 psi for 4 h and then the catalyst was filtered off and the solvent evaporated to dryness under reduced pressure to give a solid which was recrystallized.

26: yield 90%; mp 129–130 °C (cyclohexane/EtOAc); ¹H NMR 1.32 (t, 3H, Me, *J* = 7.0 Hz), 4.32 (q, 2H, CH₂, *J* = 7.0 Hz), 4.90 (s, 2H, NH₂), 7.35 (t, 1H, ar, *J* = 7.4 Hz), 7.50 (t, 2H, ar, *J* = 7.4 Hz), 7.79 (d, 2H, ar, *J* = 8.2 Hz), 7.85 (s, 1H, H5). Anal. (C₁₂H₁₃N₃O₂) C, H, N.

27: yield 78%; mp 122–124 °C (cyclohexane/EtOAc); ¹H NMR 1.31 (t, 3H, Me, *J* = 7.1 Hz), 3.80 (s, 3H, MeO), 4.30 (q, 2H, CH₂, *J* = 7.1 Hz), 4.86 (s, 2H, NH₂), 7.04 (d, 2H, ar, *J* = 9.0 Hz), 7.70 (d, 2H, ar, *J* = 9.0 Hz), 7.75 (s, 1H, H5). Anal. (C₁₃H₁₅N₃O₃) C, H, N.

28: yield 80%; mp 87–88 °C (petroleum ether 40–60 °C/diethyl ether); ¹H NMR 1.32 (t, 3H, Me, *J* = 7.1 Hz), 2.38 (s, 3H, Me), 4.31 (q, 2H, CH₂, *J* = 7.1 Hz), 4.89 (s, 2H, NH₂), 7.15 (d, 1H, ar, *J* = 7.5 Hz), 7.36 (t, 1H, ar, *J* = 7.8 Hz), 7.57 (d, 1H, *J* = 8.1 Hz), 7.63 (s, 1H, ar), 7.82 (s, 1H, H5). Anal. (C₁₃H₁₅N₃O₂) C, H, N.

General Procedure for the Synthesis of 5-Substituted 2-Arylpyrazolo[4,3-*d*]pyrimidin-7(6*H*)-ones 1, 2, 6, 12. The title compounds were prepared from ethyl 4-amino-1-arylpyrazole-3-carboxylates **26–28** (2.5 mmol), ammonium acetate (3.2 mmol), and the suitable orthoesters (3.2 mmol) under microwave irradiation at 150 °C for 15 min. The suspension was cooled at room temperature, and the solid was collected by filtration, washed with water and diethyl ether, and recrystallized. This procedure provided compounds **1** and **2** with higher yields (70% and 58%, respectively) than those obtained by the cyclization of the 4-amino-1-phenylpyrazole-3-carboxylic acid **20**, reported above.

6: yield 80%; mp 277–278 °C (acetonitrile); ¹H NMR 3.84 (s, 3H, Me), 7.12 (d, 2H, ar, *J* = 6.9 Hz), 7.84 (s, 1H, H5), 7.93 (d, 2H, ar, *J* = 6.9 Hz), 9.03 (s, 1H, H3), 11.96 (br s, 1H, NH); IR 1694. Anal. (C₁₂H₁₀N₄O₂) C, H, N.

12: yield 75%; mp 299–300 °C (2-methoxyethanol); ¹H NMR 2.31 (s, 3H, Me), 2.42 (s, 3H, Me), 7.27 (d, 1H, ar, *J* = 7.5 Hz), 7.46 (t, 1H, ar, *J* = 7.8 Hz), 7.79 (d, 1H, ar, *J* = 8.1 Hz), 7.85 (s, 1H, ar), 8.94 (s, 1H, H3), 11.90 (br s, 1H, NH); IR 1692. Anal. (C₁₃H₁₂N₄O) C, H, N.

General Procedure for the Synthesis of Ethyl 4-(2-Phenylacetamidoimido)-1-arylpyrazole-3-carboxylate Hydrochlorides 29 and 30. Dry hydrogen chloride was bubbled for about 30 min through a mixture of phenylacetoneitrile (4.4 mmol) and ethyl 4-amino-1-arylpyrazole-3-carboxylate **26** or **27** (2.2 mmol) in anhydrous dioxane (20 mL). The mixture was stirred at room temperature for a further 3–4 h. Then the solid was collected by filtration and washed with diethyl ether. Crude compounds **29** and **30** were not recrystallized but were directly used for the next step.

29: yield 60%; ¹H NMR 1.18 (t, 3H, Me, *J* = 7.1 Hz), 4.08 (s, 2H, benzyl CH₂), 4.12 (q, 2H, CH₂), 7.33–7.46 (m, 4H, ar), 7.58 (t, 2H, ar, *J* = 7.4 Hz), 7.71 (d, 2H, ar, *J* = 7.6 Hz), 7.91 (d, 2H, ar, *J* = 7.4 Hz), 8.91 (br s, 1H, NH), 8.98 (s, 1H, H5), 10.23 (s, 1H, NH₂⁺ proton), 12.00 (s, 1H, NH₂⁺ proton).

30: yield 80%; ¹H NMR 1.18 (t, 3H, Me, *J* = 7.2 Hz), 3.83 (s, 3H, OMe), 4.02 (s, 2H, benzyl CH₂), 4.18 (q, 2H, CH₂, *J* = 7.2 Hz), 7.12 (d, 2H, ar, *J* = 7.0 Hz), 7.37–7.43 (m, 3H, ar), 7.60 (d, 2H, ar, *J* = 6.9 Hz), 7.83 (d, 2H, ar, *J* = 7.0 Hz), 8.87 (s, 1H, H5), 8.91 (br s, 1H, NH), 10.00 (br s, 1H, NH₂⁺ proton), 11.62 (br s, 1H, NH₂⁺ proton).

General Procedure for the Synthesis of 2-Aryl-5-benzylpyrazolo[4,3-*d*]pyrimidin-7(6*H*)-ones 5 and 10. Intermediates **29** and **30** were heated at 230 °C under nitrogen atmosphere for about 1–2 h. Compound **5** was purified by recrystallization from ethanol, while derivative **10** was chromatographed on silica gel column (eluent, cyclohexane/EtOAc, 2:8) and then recrystallized from 2-methoxyethanol.

5: yield 75%; mp > 300 °C; ¹H NMR 3.92 (s, 2H, CH₂), 7.23–7.38 (m, 5H, ar), 7.44 (t, 1H, ar, *J* = 7.6 Hz), 7.59 (t, 2H, ar, *J* = 7.7 Hz), 7.91 (d, 2H, ar, *J* = 8.2 Hz), 9.03 (s, 1H, H3), 12.13 (br s, 1H, NH); IR 1702. Anal. (C₁₈H₁₄N₄O) C, H, N.

10: yield 55%; mp 293 °C dec; ¹H NMR 3.83 (s, 3H, OMe), 3.91 (s, 2H, CH₂), 7.13 (d, 2H, ar, *J* = 8.8 Hz), 7.23–7.37 (m, 5H, ar), 7.89 (d, 2H, ar, *J* = 8.9 Hz), 8.91 (s, 1H, H3), 12.09 (br s, 1H, NH); IR 1673. Anal. (C₁₉H₁₆N₄O₂) C, H, N.

Synthesis of 4-Nitro-2-phenylpyrazole-4-carboxamide 31. A stream of ammonia was bubbled through a suspension of the ester **23** (3.0 mmol) in 33% aqueous ammonia solution (40 mL) for about 2 h. Then the suspension was stirred at room temperature for an additional 6 h. The solid was collected by filtration, washed with water, and recrystallized from 2-ethoxyethanol. Yield 85%; mp 230–232 °C; ¹H NMR 7.24 (t, 1H, ar, *J* = 7.3 Hz), 7.59 (t, 2H, ar, *J* = 6.9 Hz), 7.90 (br s, 1H, NH₂ amide proton), 7.96 (d, 2H, ar, *J* = 7.6 Hz), 8.18 (br s, 1H, NH₂ amide proton), 9.64 (s, 1H, H5). Anal. (C₁₀H₈N₄O₃) C, H, N.

Synthesis of 4-Amino-2-phenylpyrazole-4-carboxamide 32.²² The nitro derivative **31** (2.0 mmol) was dissolved in boiling ethanol (about 150 mL), and 10% Pd/C (0.05 g) was added to the solution. The mixture was hydrogenated in a Parr apparatus at 35 psi for 4 h. The catalyst was filtered off and the solvent evaporated at reduced pressure to give an oil that spontaneously solidified. Yield 60%; mp 196–198 °C (MeOH), (lit. 189–191 °C);²² ¹H NMR 4.86 (s, 2H, NH₂), 7.24 (br s, 1H, NH₂ proton), 7.29 (t, 1H, ar, *J* = 7.4 Hz), 7.46–7.50 (m, 3H, 2ar + NH₂ proton), 7.79 (s, 1H, H5), 7.83 (d, 2H, ar, *J* = 8.7 Hz). Anal. (C₁₀H₁₀N₄O) C, H, N.

Synthesis of 2-Phenylpyrazolo[4,3-*d*]pyrimidin-5,7-(4*H*,6*H*)-dione 13. A solution of triethylamine (2.16 mmol) in anhydrous tetrahydrofuran (3 mL) was added dropwise to a mixture of compound **32** (0.92 mmol) and triphosgene (0.36 mmol) in anhydrous tetrahydrofuran (20 mL). The mixture was refluxed for 8 h, then cooled at room temperature and diluted with ice–water. The solid was collected by filtration, washed with water, and recrystallized from dimethylformamide. Yield 55%; mp > 300 °C; ¹H NMR 7.41 (t, 1H, ar, *J* = 7.4 Hz), 7.55 (t, 2H, ar, *J* = 7.6 Hz), 7.95 (d, 2H, ar, *J* = 7.8 Hz), 11.03 (br s, 1H, NH), 11.09 (br s, 1H, NH); IR 1715, 1748, 3059, 3150. Anal. (C₁₁H₈N₄O₂) C, H, N.

(B) Computational Methodologies. All modeling studies were carried out on a 20 CPU (Intel Core2 Quad CPU 2.40 GHz) Linux cluster. Homology modeling, energy calculation, and analyses of docking poses were performed using the Molecular Operating Environment (MOE, version 2008.10) suite.³⁵ The software package MOPAC (version 7),³⁶ implemented in the MOE suite, was utilized for all quantum mechanical calculations. Docking simulations were performed using the GOLD suite.³⁷

Homology Model of the hA₃ AR. On the basis of the assumption that GPCRs share similar TM boundaries and overall topology, a homology model of the hA₃ adenosine receptor was constructed using as template the recently published crystal structure of the hA_{2A} receptor.²¹ In Figure 4, we show the alignment of the aminoacidic sequences of the two human adenosine receptors considered in our study (hA₃/hA_{2A} sequence identity of ~42%).

		N-term	TM1	IL1	TM2		
hA3 (P33765)		MPNNSTAL	SLANVTYITMEIFIGLCAIVGNVLVICVVKLNPSLQT	TTFFYFIVSLALADIA		60	
hA2A (P29274)		MP-----	IMGSSVYITVELAIAVLAILGNVLVCWAVLNSNLQNV	TNYFVVSLLAAADIA		54	
		**	*** *	* ** *	*** ** *		
		EL1	TM3	IL2			
hA3 (P33765)		VGVLVMP	LAIVVSLGITIHFYSCLFMTCLLLIFTHASIMSLLAIAVDRLRV	KLTVRYKR		120	
hA2A (P29274)		VGVLAI	PFATISTGFCACHGCLFIACFVLVLTQSSIFSLLAIAIDRYIAIRI	PLRYNG		114	
		**** *	*** *	*** ** *	**		
		TM4	EL2				
hA3 (P33765)		VTTHRR	IWLALGLCWLVSFLVGLTPMF	GWNMKLTSE-----YHRNV	TFLSCQFVSVMRM	174	
hA2A (P29274)		LVTGT	RAKGIIAICWVLSFAIGLTPML	GWNNCGQPKEGKNHSQGC	GEGQVACLFEDVVP	174	
		* *	** ** *	***** *	* ** *		
		TM5	IL3				
hA3 (P33765)		DYMVYFS	FLTWFIFLPLVVMCAIYLDIF	YIIRNKLSLNLN---	SKETGAFY	GREFKTAKS 231	
hA2A (P29274)		NYMVYFN	FFACVLVPLLLMLGVYLRIF	LAARRQLKQMESQPLP	GERARSTL	QKEVHA	AKS 234
		***** *	** *	*** ** *	* ** *		
		TM6	EL3	TM7			
hA3 (P33765)		LFLVLFL	FALSWLPLSIINCIIFYN---	GEVPLVLV	MGILLSHANSMMNP	IVYAYKIKK 288	
hA2A (P29274)		LAIIVGL	FALCWLPLHIINCF	TFFCPDCSHAPLWLMY	LAIVLSHTNSV	VNPFYAYRIRE 294	
		*	**** *	*** ** *	* ** *	*** *	
		C-term					
hA3 (P33765)		FKETYLL	IILKACVV-----	CHPSDSL	DTSIEKNSE-----	318	
hA2A (P29274)		FRQTR	KIIRSHVLRQQEPFKAAGTSARV	LAHGS	DGEQVSLRLNGHPP	GVWANGSAPHP 354	
		* * *	*	*** *	* *		
hA3 (P33765)		-----					
hA2A (P29274)		ERRP	NGYALGLVSGGSAQESQ	GNTGLPDV	ELLSHELKGV	CPPEPGLDDPLA	QDGAGVS 412

Figure 4. Sequence alignment of hA₃ and hA_{2A} ARs. Conserved residues are identified by asterisks.

The numbering of the amino acids in parentheses follows the arbitrary scheme by Ballesteros and Weinstein. According to this scheme, each amino acid identifier starts with the helix number, followed by the position relative to a reference residue among the most conserved amino acid in that helix. The number 50 is arbitrarily assigned to the reference residue.³⁸

First, the amino acid sequences of TM helices of the hA₃ receptor were aligned with those of the template, guided by the highly conserved amino acid residues, including the DRY motif (Asp3.49, Arg3.50, and Tyr3.51) and three proline residues (Pro4.60, Pro6.50, and Pro7.50) in the TM segments of GPCRs. The same boundaries were applied for the TM helices of the hA₃ receptor as they were identified from the 3D structure for the corresponding sequences of the template, the coordinates of which were used to construct the seven TM helices for the hA₃ receptor. The loop domains were constructed by the loop search method implemented in MOE on the basis of the structure of compatible fragments found in the Protein Data Bank. In particular, loops are modeled first in random order. For each loop, a contact energy function analyzes the list of candidates collected in the segment searching stage, taking into account all atoms already modeled and any atoms specified by the user as belonging to the model environment. These energies are then used to make a Boltzmann-weighted choice from the candidates, the coordinates of which are then copied to the model. Side chains were modeled using a library of rotamers generated by systematic clustering of the Protein Data Bank data, using the same procedure. Side chains belonging to residues, whose backbone coordinates were copied from a template, are modeled first, followed by side chains of modeled loops. Outgaps and their side chains are modeled last. Special caution has to be given to EL2 because amino acids of this loop could be involved in direct interactions with the ligands. A driving force to the peculiar fold of the EL2 loop might be the presence of a disulfide

bridge between cysteines in TM3 and EL2. Since this covalent link is conserved in all receptors considered in the current study, the EL2 loop was modeled using a constrained geometry around the EL2–TM3 disulfide bridge. The constraints were applied before the construction of the homology model, in particular during the sequences alignment. The cysteine residues, involved in the disulfide bridge in the hA_{2A} receptor, were selected to be constrained with the corresponding cysteines in the hA₃ receptor sequence. In particular, Cys166 (EL2) and Cys77 (3.25) of the hA_{2A} receptor were constrained, respectively, with Cys166 (EL2) and Cys83 (3.25) of the hA₃ receptor. During the alignment, MOE-Align attempts to minimize the number of constraint violations. Then, after running the homology modeling, the presence of the conserved disulfide bridge in the model was manually checked. After the heavy atoms were modeled, all hydrogen atoms were added and were then minimized with MOE using the AMBER99 force field.³⁹ The minimizations were carried out by the 1000 steps of steepest descent followed by conjugate gradient minimization until the rms gradient of the potential energy was less than 0.1 kcal mol⁻¹ Å⁻¹. We used the Protonate 3D methodology, part of the MOE suite, for protonation state assignment by selecting a protonation state for each chemical group that minimizes the total free energy of the system (taking titration into account).⁴⁰

Protein stereochemistry evaluation was then performed by several tools (Ramachandran and χ plots measure ϕ/ψ and χ_1/χ_2 angles, clash contacts reports) implemented in the MOE suite.³⁵

Molecular Docking of hA₃ AR Antagonists. Ligand structures were built using the MOE-builder tool, part of the MOE suite,³⁵ and were subjected to MMFF94x energy minimization until the rms of conjugate gradient was 0.05 kcal mol⁻¹ Å⁻¹. Charges were calculated using PM3/ESP methodology.

Four different programs were used to calibrate our docking protocols: MOE-Dock,³⁵ GOLD,³⁷ Glide,⁴¹ and PLANTS.⁴²

ZM-241385 was redocked to the crystal structure of the hA_{2A} AR (PDB code 3EML) with different docking algorithms and scoring functions (see Table 3). Each docking was performed automatically to the binding site of the hA_{2A} AR without any constraints and without the presence of water molecules. For all the different docking simulations, the center of the docking box or of the docking sphere was set in the same point (obtained from the experimental pose of ZM-241385 inside the crystal structure of hA_{2A} AR), and the number of independent docking runs was set to 25. Then rmsd values between predicted and crystallographic positions of ZM-241385 were calculated.

As shown in Table 2, for each docking result there is at least one pose in good agreement with the experimental binding mode (rmsd value of <2.5 Å). These poses with the lowest rmsd value differ from the crystallographic pose of ZM-241385 mainly in the position of the phenylethylamine chain, while the bicyclic triazolotriazine core is almost aligned. However, the mean rmsd value is quite high for most of the docking protocols tested except for Gold. Docking performed with Gold gives the lowest rmsd value, the lowest mean rmsd value, and the highest number of poses with rmsd value of <2.5 Å.

On the basis of the best docking performance, all antagonist structures were docked into the hypothetical TM binding site of the hA₃ AR model and of the crystal structure of the hA_{2A} AR, by using the dock tool part of the GOLD suite.³⁷ Searching is conducted within a user-specified docking sphere, using the Genetic Algorithm protocol and the GoldScore scoring function. GOLD performs a user-specified number of independent docking runs (25 in our specific case) and writes the resulting conformations and their energies in a molecular database file. The resulting docked complexes were subjected to MMFF94x energy minimization until the rms of the conjugate gradient was <0.1 kcal mol⁻¹ Å⁻¹. Charges for the ligands were imported from the MOPAC output files using PM3/ESP methodology.

Prediction of the antagonist–receptor complex stability (in terms of corresponding pK_i value) and the quantitative analysis for nonbonded intermolecular interactions (H-bonds, transition metal, water bridges, hydrophobic, electrostatic) were calculated and visualized using several tools implemented in the MOE suite.³⁵

Electrostatic contributions to the binding energy of individual amino acids have been calculated as implemented in the MOE suite.³⁵ To estimate the electrostatic contributions, atomic charges for the ligands were calculated using PM3/ESP methodology. Partial charges for protein amino acids were calculated on the basis of the AMBER99 force field.

(C) Pharmacological Assays. Human Cloned A₁, A_{2A}, and A₃ AR Binding Assay. All synthesized compounds were tested to evaluate their affinity at human A₁, A_{2A}, and A₃ adenosine receptors. Displacement experiments of [³H]DPCPX (1 nM) to hA₁ CHO membranes (50 µg of protein/assay) and at least six to eight different concentrations of antagonists for 120 min at 25 °C in 50 mM Tris HCl buffer, pH 7.4, were performed.⁴³ Nonspecific binding was determined in the presence of 10 µM CHA (≤10% of the total binding). Binding of [³H]ZM-241385 (1 nM) to hA_{2A} CHO membranes (50 µg of protein/assay) was performed by using 50 mM Tris-HCl buffer and 10 mM MgCl₂, pH 7.4, and at least six to eight different concentrations of antagonists were studied for an incubation time of 60 min at 4 °C.⁴⁴ Nonspecific binding was determined in the presence of 1 µM ZM-241385 and was about 20% of total binding. Competition binding experiments to hA₃ CHO membranes (50 µg of protein/assay) and 0.5 nM [¹²⁵I]AB-MECA, 50 mM Tris HCl buffer, 10 mM MgCl₂, 1 mM EDTA, pH 7.4, were conducted, and at least six to eight different concentrations of examined ligands were studied for 120 min at 4 °C.⁴⁵ Nonspecific binding was defined as binding in the presence of 1 µM AB-MECA and was about 20% of total binding. Bound and free radioactivity were separated by filtering the assay mixture through Whatman GF/B glass fiber filters by using a Brandel cell harvester. The filter bound

radioactivity was counted by a Packard Tri Carb 2500 TR scintillation counter with an efficiency of 58%.

Measurement of Cyclic AMP Levels in CHO Cells Transfected with hA_{2B} or hA₃ AR. CHO cells transfected with hAR subtypes were washed with phosphate-buffered saline and diluted trypsin and centrifuged for 10 min at 200g. The pellet containing the CHO cells (1 × 10⁶ cells/assay) was suspended in 0.5 mL of incubation mixture (mM): NaCl 15, KCl 0.27, NaH₂PO₄ 0.037, MgSO₄ 0.1, CaCl₂ 0.1, Hepes 0.01, MgCl₂ 1, glucose 0.5, pH 7.4 at 37 °C, 2 IU/mL adenosine deaminase and 4-(3-butoxy-4-methoxybenzyl)-2-imidazolidinone (Ro 20-1724) as phosphodiesterase inhibitor and preincubated for 10 min in a shaking bath at 37 °C. The potency of antagonists to the A_{2B} AR was determined by antagonism of NECA (200 nM) induced stimulation of cyclic AMP levels. In addition, the potency of antagonists to the A₃ receptor was determined in the presence of 1 µM forskolin and 100 nM Cl-IB-MECA that mediated inhibition of cyclic AMP levels. The reaction was terminated by the addition of cold 6% trichloroacetic acid (TCA). The TCA suspension was centrifuged at 2000g for 10 min at 4 °C, and the supernatant was extracted four times with water-saturated diethyl ether. The final aqueous solution was tested for cyclic AMP levels by a competition protein binding assay. Samples of cyclic AMP standard (0–10 pmol) were added to each test tube containing [³H]cAMP and the incubation buffer (0.1 M trizma base, 8.0 mM aminophylline, 6.0 mM 2-mercaptoethanol, pH 7.4). The binding protein prepared from beef adrenals was added to the samples previously incubated at 4 °C for 150 min and, after the addition of charcoal, was centrifuged at 2000g for 10 min. The clear supernatant was counted in a Packard Tri Carb 2500 TR scintillation counter with an efficiency of 58%.⁴⁶

Data Analysis. The protein concentration was determined according to a Bio-Rad method⁴⁷ with bovine albumin as a standard reference. Inhibitory binding constant (K_i) values were calculated from IC₅₀ according to the Cheng and Prusoff equation $K_i = IC_{50}/(1 + [C^*]/K_D^*)$, where [C*] is the concentration of the radioligand and K_D* its dissociation constant.⁴⁸ A weighted nonlinear least-squares curve-fitting program LI-GAND⁴⁹ was used for computer analysis of inhibition experiments. EC₅₀ and IC₅₀ values obtained in a cyclic AMP assay were calculated by nonlinear regression analysis using the equation for a sigmoid concentration–response curve (GraphPAD Prism, San Diego, CA).

Acknowledgment. The synthetic work was supported by a grant of the Italian Ministry for University and Research (MIUR, FIRB RBNE03YA3L Project). The molecular modeling work coordinated by S.M. was carried out with financial support from the University of Padova, Italy, and the Italian Ministry for University and Research (MIUR), Rome, Italy. S.M. is also very grateful to Chemical Computing Group for the scientific and technical partnership.

Supporting Information Available: Combustion analysis data of the synthesized compounds. This material is available free of charge via the Internet at <http://pubs.acs.org>.

References

- (1) Fredholm, B. B.; IJzerman, A. P.; Jacobson, K. A.; Klotz, K. N.; Linden, J. International Union of Pharmacology XXV. Nomenclature and classification of adenosine receptors. *Pharmacol. Rev.* **2001**, *53*, 527–552.
- (2) Jacobson, K. A.; Knutsen, L. J. S. P1 and P2 Purine and Pyrimidine Receptor Ligands. In *Purinergic and Pyrimidinergic Signalling*; Abbracchio, M. P., Williams, M., Eds; Handbook of Experimental Pharmacology, Vol. 151/1; Springer: Berlin, 2001; pp 129–175.
- (3) Abbracchio, M. P.; Brambilla, R.; Kim, H. O.; von Lubitz, D. K. J. E.; Jacobson, K. A.; Cattabeni, F. G-Protein-dependent activation of phospholipase-C by adenosine A₃ receptor in rat brain. *Mol. Pharmacol.* **1995**, *48*, 1083–1045.

- (4) Ali, H.; Choi, O. H.; Fraundorfer, P. F.; Yamada, K.; Gonzaga, H. M. S.; Beaven, M. A. Sustained activation of phospholipase-D via adenosine A₃ receptors is associated with enhancement of antigen-ionophore-induced and Ca²⁺-ionophore-induced secretion in a rat mast-cell line. *J. Pharmacol. Exp. Ther.* **1996**, *276*, 837–845.
- (5) Shneyvays, V.; Leshem, D.; Zinman, T.; Mamedova, L. K.; Jacobson, K. A.; Shainberg, A. Role of adenosine A₁ and A₃ receptors in regulation of cardiomyocyte homeostasis after mitochondrial respiratory chain injury. *Am. J. Physiol.: Heart Circ. Physiol.* **2005**, *288*, H2792–H2801.
- (6) Englert, M.; Quitterer, U.; Klotz, K. N. Effector coupling of stably transfected human A₃ adenosine receptor in CHO cells. *Biochem. Pharmacol.* **2002**, *64*, 61–65.
- (7) Schulte, G.; Fredholm, B. B. Signalling from adenosine receptors to mitogen-activated protein kinases. *Cell. Signalling* **2003**, *15*, 813–827.
- (8) Brambilla, R.; Cattabeni, F.; Ceruti, S.; Barbieri, D.; Franceschi, C.; Kim, Y.-C.; Jacobson, K. A.; Klotz, K.-N.; Lohse, M. J.; Abbracchio, M. P. Activation of the A₃ adenosine receptor affect cell cycle progression and cell growth. *Naunyn-Schmiedeberg's Arch. Pharmacol.* **2000**, *361*, 225–234.
- (9) Gessi, S.; Merighi, S.; Varani, K.; Leung, E.; Mac Lennan, S.; Borea, P. A. The A₃ adenosine receptor: an enigmatic player in cell biology. *Pharmacol. Ther.* **2008**, *117*, 123–140.
- (10) Merighi, S.; Mirandola, P.; Varani, K.; Gessi, S.; Leung, E.; Baraldi, P. G.; Tabrizi, M. A.; Borea, P. A. A glance at adenosine receptors: a novel target for antitumor therapy. *Pharmacol. Ther.* **2003**, *100*, 31–48.
- (11) Merighi, S.; Benini, A.; Mirandola, P.; Gessi, S.; Varani, K.; Leung, E.; MacLennan, S.; Borea, P. A. Adenosine modulates vascular endothelial growth factor expression via hypoxia-inducible factor-1 in human glioblastoma cells. *Biochem. Pharmacol.* **2006**, *72*, 19–31.
- (12) Colotta, V.; Catarzi, D.; Varano, F.; Cecchi, L.; Filacchioni, G.; Martini, C.; Trincavelli, L.; Lucacchini, A. 1,2,4-Triazolo[4,3-*a*]quinoxalin-1-one: a versatile tool for the synthesis of potent and selective adenosine receptor antagonists. *J. Med. Chem.* **2000**, *43*, 1158–1164.
- (13) Colotta, V.; Catarzi, D.; Varano, F.; Cecchi, L.; Filacchioni, G.; Martini, C.; Trincavelli, L.; Lucacchini, A. Synthesis and structure–activity relationships of a new sets of 2-arylpyrazolo[3,4-*c*]quinoline derivatives as adenosine receptor antagonists. *J. Med. Chem.* **2000**, *43*, 3118–3124.
- (14) Colotta, V.; Catarzi, D.; Varano, F.; Calabri, F. R.; Lenzi, O.; Filacchioni, G.; Trincavelli, L.; Martini, C.; Deflorian, F.; Moro, S. 1,2,4-Triazolo[4,3-*a*]quinoxalin-1-one moiety as an attractive scaffold to develop new potent and selective human A₃ adenosine receptor antagonists: synthesis, pharmacological and ligand–receptor modeling studies. *J. Med. Chem.* **2004**, *47*, 3580–3590.
- (15) Catarzi, D.; Colotta, V.; Varano, F.; Lenzi, O.; Filacchioni, G.; Trincavelli, L.; Martini, C.; Montopoli, C.; Moro, S. 1,2,4-Triazolo[1,5-*a*]quinoxaline as a versatile tool for the design of selective human A₃ adenosine receptor antagonists: synthesis, biological evaluation and molecular modeling studies of 2-(hetero)aryl- and 2-carboxy-substituted derivatives. *J. Med. Chem.* **2005**, *48*, 7932–7945.
- (16) Lenzi, O.; Colotta, V.; Catarzi, D.; Varano, F.; Filacchioni, G.; Martini, C.; Trincavelli, L.; Ciampi, O.; Marighetti, F.; Morizzo, E.; Moro, S. 4-Amido-2-aryl-1,2,4-triazolo[4,3-*a*]quinoxalin-1-ones as new potent and selective human A₃ adenosine receptor antagonists. Synthesis, pharmacological evaluation and ligand–receptor modeling studies. *J. Med. Chem.* **2006**, *49*, 3916–3925.
- (17) Colotta, V.; Catarzi, D.; Varano, F.; Capelli, F.; Lenzi, O.; Filacchioni, G.; Martini, C.; Trincavelli, L.; Ciampi, O.; Pugliese, A. M.; Pedata, F.; Schiesaro, A.; Morizzo, E.; Moro, S. New 2-arylpyrazolo[3,4-*c*]quinoline derivatives as potent and selective human A₃ adenosine receptor antagonists: synthesis, pharmacological evaluation, and ligand–receptor modeling studies. *J. Med. Chem.* **2007**, *50*, 4061–4074.
- (18) Morizzo, E.; Capelli, F.; Lenzi, O.; Catarzi, D.; Varano, F.; Filacchioni, G.; Vincenzi, F.; Varani, K.; Borea, P. A.; Colotta, V.; Moro, S. Scouting human A₃ adenosine receptor antagonist binding mode using a molecular simplification approach: from triazoloquinoxaline to a pyrimidine skeleton as a key study. *J. Med. Chem.* **2007**, *50*, 6596–6606.
- (19) Colotta, V.; Capelli, F.; Lenzi, O.; Catarzi, D.; Varano, F.; Poli, D.; Vincenzi, F.; Varani, K.; Borea, P. A.; Ben, Dal; Volpini, D.; Cristalli, R.; Filacchioni, G. Novel potent and highly selective human A₃ adenosine receptor antagonists belonging to the 4-amido-2-arylpyrazolo[3,4-*c*]quinoline series: molecular docking analysis and pharmacological studies. *Bioorg. Med. Chem.* **2009**, *17*, 401–410.
- (20) Colotta, V.; Lenzi, O.; Catarzi, D.; Varano, F.; Filacchioni, G.; Martini, C.; Trincavelli, L.; Ciampi, O.; Pugliese, A. M.; Traini, C.; Pedata, F.; Schiesaro, A.; Morizzo, E.; Moro, S. Pyrido[2,3-*e*]1,2,4-triazolo[4,3-*a*]pyrazin-1-one as a new scaffold to develop potent and selective human A₃ adenosine receptor antagonists. Pharmacological evaluation, and ligand–receptor modeling studies. *J. Med. Chem.* **2009**, *52*, 2407–2419.
- (21) Jaakola, V. P.; Griffith, M. T.; Hanson, M. A.; Cherezov, V.; Chien, E. Y. T.; Lane, J. R.; IJzerman, A. P.; Stevens, R. C. The 2.6 angstrom crystal structure of a human A_{2A} adenosine receptor bound to an antagonist. *Science* **2008**, *322*, 1211–1217.
- (22) Gewald, K.; Calderon, O. 4-Amino-1-arylpyrazole durch Thorpecyclisierung. *Monatsh. Chem.* **1977**, *108*, 611–616.
- (23) Fevig, J. M.; Cacciola, J.; Buriak, J., Jr.; Rossi, K. A.; Knabb, R. M.; Luetting, J. M.; Wong, P. C.; Bai, S. A.; Wexler, R. R.; Lam, P. Y. S. Preparation of 1-(4-methoxyphenyl)-1*H*-pyrazolo[4,3-*d*]pyrimidin-7(6*H*)-ones as potent selective and bioavailable inhibitors of coagulation factor Xa. *Bioorg. Med. Chem. Lett.* **2006**, *16*, 3755–3760.
- (24) Desai, N. D.; Shah, R. D. Improved protocol for Thorpe reaction: synthesis of 4-amino-1-arylpyrazole using solid–liquid phase-transfer conditions. *Synth. Commun.* **2008**, *38*, 316–327.
- (25) Nicolaou, K. C.; Snyder, S. A.; Huang, X.; Simonsen, K. B.; Koumbis, A. E.; Bigot, A. Studies toward diazonamide A: initial synthetic forays directed toward the originally proposed structure. *J. Am. Chem. Soc.* **2004**, *126*, 10162–10173.
- (26) Shawali, A. S.; Albar, H. A. Kinetics and mechanism of dehydrochlorination of *N*-aryl-*C*-ethoxycarbonylformohydrazidoyl chlorides. *Can. J. Chem.* **1986**, *64*, 871–875.
- (27) Lozinskii, M. O.; Kukota, S. N.; Pel'kis, P. S. Ethyl arylazochloroacetates and their reactions with morpholine and hydrazine hydrate. *Ukr. Khim. Zh.* **1967**, *33*, 1295–1296 [Chem. Abstr. 1968, 69, 51762].
- (28) Hassaneen, H. M. E.; Hassaneen, H. M.; Elnagdi, M. H. Enamines in heterocyclic synthesis: a route to 4-substituted pyrazoles and condensed pyrazoles. *Z. Naturforsch., B: Chem. Sci.* **2004**, *59*, 1132–1136.
- (29) Palczewski, K.; Kumasaka, T.; Hori, T.; Behnke, C. A.; Motoshima, H.; et al. Crystal structure of rhodopsin: a G protein-coupled receptor. *Science* **2000**, *289*, 739–745.
- (30) Rosenbaum, D.; Cherezov, V.; Hanson, M.; Rasmussen, S.; Thian, F.; Kobilka, T.; Choi, H.; Yao, X.; Weis, W.; Stevens, R.; Kobilka, B. GPCR engineering yields high-resolution structural insights into beta2-adrenergic receptor function. *Science* **2007**, *318*, 1266–1273.
- (31) Scholl, D. J.; Wells, J. N. Serine and alanine mutagenesis of the nine native cysteine residues of the human A₁(I) adenosine receptor. *Biochem. Pharmacol.* **2000**, *60*, 1647–1654.
- (32) Kim, J.; Wess, J.; van Rhee, M.; Schoneberg, T.; Jacobson, K. A. Site-directed mutagenesis identifies residues involved in ligand recognition in the human A_{2A} adenosine receptor. *J. Biol. Chem.* **1995**, *270*, 13987–13997.
- (33) Gao, Z.-G.; Chen, A.; Barak, D.; Kim, S.-K.; Muller, C. E.; Jacobson, K. A. Identification by site-directed mutagenesis of residues involved in ligand recognition and activation of the human A₃ adenosine receptor. *J. Biol. Chem.* **2002**, *277*, 19056–19063.
- (34) Kim, J.; Jiang, Q.; Glashofer, M.; Yehle, S.; Wess, J.; Jacobson, K. A. Glutamate residues in the second extracellular loop of the human A_{2a} adenosine receptor are required for ligand recognition. *Mol. Pharmacol.* **1996**, *49*, 683–691.
- (35) MOE (Molecular Operating Environment), version 2008.10; Chemical Computing Group Inc. (1010 Sherbrooke Street West, Suite 910, Montreal, Quebec H3A 2R7, Canada); <http://www.chemcomp.com>.
- (36) Stewart, J. J. P. *MOPAC 7*; Fujitsu Limited: Tokyo, 1993.
- (37) GOLD Suite, version 4.0.1; Cambridge Crystallographic Data Centre Cambridge Crystallographic Data Centre (12 Union Road, Cambridge CB2 1EZ, U.K.); <http://www.ccdc.cam.ac.uk>
- (38) Ballesteros, J. A.; Weinstein, H. Integrated methods for the construction of three-dimensional models and computational probing of structure-function relationships in G-protein coupled receptors. *Methods Neurosci.* **1995**, *25*, 366–428.
- (39) Wang, J.; Cieplack, P.; Kollman, P. A. *J. Comput. Chem.* **2000**, *21*, 1049–1074.
- (40) Labute, P. Protonate3D: Assignment of ionization states and hydrogen coordinates to macromolecular structures. *Proteins* **2009**, *75*, 187–205.
- (41) Halgren, T. A.; Myrphy, R. B.; Friesner, R. A.; Beard, H. S.; Frye, L. L.; Pollard, W. T. Glide: a new approach for rapid, accurate docking and scoring 1 methods and assessment of docking accuracy. *J. Med. Chem.* **2004**, *47*, 1739–1749.

- (42) Korb, O.; Stutzle, T.; Exner, T. E. Empirical scoring functions for advanced protein–ligand docking with PLANTS. *J. Chem. Inf. Model.* **2009**, *49*, 84–96.
- (43) Borea, P. A.; Dalpiaz, A.; Varani, K.; Gessi, S.; Gilli, G. Binding thermodynamics at A₁ and A_{2A} adenosine receptors. *Life Sci.* **1996**, *59*, 1373–1388.
- (44) Varani, K.; Rigamonti, D.; Sipione, S.; Camurri, A.; Borea, P. A.; Cattabeni, F.; Abbraccio, M. P.; Cattaneo, E. Aberrant amplification of A_{2A} receptor signalling in striatal cells expressing mutant huntigtin. *FASEB J.* **2001**, *5*, 1245–1247.
- (45) Varani, K.; Cacciari, B.; Baraldi, P. G.; Dionisotti, S.; Ongini, E.; Borea, P. A. Binding affinity of adenosine receptor agonists and antagonists at human cloned A₃ adenosine receptors. *Life Sci.* **1998**, *63*, 81–87.
- (46) Varani, K.; Gessi, S.; Merighi, S.; Vincenzi, F.; Cattabriga, E.; Benini, A.; Klotz, K.-N.; Baraldi, P. G.; Tabrizi, M.-A.; Mac Lennan, S.; Leung, E.; Borea, P. A. Pharmacological characterization of novel adenosine ligands in recombinant and native human A_{2B} receptors. *Biochem. Pharmacol.* **2005**, *70*, 1601–1612.
- (47) Bradford, M. M. A rapid and sensitive method for the quantification of microgram quantities of protein utilizing the principle of protein-dye binding. *Anal. Biochem.* **1976**, *72*, 248–254.
- (48) Cheng, Y. C.; Prusoff, W. H. Relationships between the inhibition constant (K_i) and the concentration of inhibitor which causes 50% inhibition (IC_{50}) of an enzymatic reaction. *Biochem. Pharmacol.* **1973**, *22*, 3099–3108.
- (49) Munson, P. J.; Rodbard, D. Ligand: a versatile computerized approach for the characterization of ligand binding systems. *Anal. Biochem.* **1980**, *107*, 220–239.